공학석사 학위논문

Development of Electron Temperature Diagnostics Using Soft X-ray Absorber Foil Method in Versatile Experiment Spherical Torus (VEST)

연 엑스선 박막 흡수 방법을 이용한 VEST 장치에서의 전자온도 진단 시스템 개발

2014년 2월

서울대학교 대학원

에너지시스템공학부

조 정 민

Development of Electron Temperature Diagnostics by Using Soft X-ray Absorber Foil Method in Versatile Experiment Spherical Torus (VEST)

지도교수 황 용 석

이 논문을 공학석사 학위논문으로 제출함
2014년 1월

서울대학교 대학원
에너지시스템공학부
조정민

조정민의 석사 학위논문을 인준함
2014년 2월

위 원 장 나 용 수 (인)

부위원장 황 용 석 (인)

위 원 정 경 재 (인)

Abstract

Development of Electron Temperature Diagnostics by Using Soft X-ray Absorber Foil Method in Versatile Experiment Spherical Torus (VEST)

Jungmin Jo

Department of Energy System Engineering

The Graduate School

Seoul National University

Electron temperature diagnostics using SXR (soft X-ray) absorber foil method has been developed to measure line averaged electron temperature of the VEST (Versatile Experiment Spherical Torus) at Seoul National University. SXR absorber foil method is relatively simple method to diagnose line averaged electron temperature, which is measured by the ratio of transmitted radiation intensity between two different thickness foils. It has very good time resolutions so it can be useful to detect various phenomena. Also it can be a

complementary diagnostics of other electron temperature diagnostics such as Thomson scattering system.

The expected electron temperature of the VEST core plasmas is about one hundred eV. In order to measure temperatures in this range, aluminum foils with thicknesses of 0.8 μm and 1.5 μm aluminum foils are chosen by calculating the variations of intensity ratio and signal strength according to electron temperature. Each foil is located in front of detectors which are installed in the midplane of the VEST chamber to diagnose core plasmas. AXUV-16ELG photodiode is employed as a detector in favor of its good responsivity in the SXR region. Each signal lines are twisted and carefully shielded with copper braided wires which can reject electromagnetic noises.

This diagnostic method can be affected by impurity line radiation and non-thermal radiations generated by runaway electrons, so it is important to know the amount and causes of these radiations. Calculations are performed to estimate these radiation effects. From this calculation if there is oxygen line radiation which is considered as a major impurity in VEST overestimates or underestimates in measured electron temperature is expected according to its value. If there is non-thermal high energy radiations underestimated electron temperature is expected. To estimate intensity of these radiations two experimental components are prepared. Bandpass filter around 780 nm is used for monitoring the evolution of oxygen atom and an additional thick aluminum foil is used to see the effect of the non-thermal high energy photons. With these calculation and experimental setup H-alpha line signal and triple Langmuir probe are also used for the interpretation of experimental results.

To see the performance of the diagnostics test experiments are performed in ECH (Electron Cyclotron Heating) pre-ionized ohmic plasmas in VEST. In the first test experiments the electron temperature at the plasma current peak is about 110 eV and this value sustained almost the same during the plasma ramp down phase. In the latter part of the discharge large uncertainties are expected in measured electron temperature due to the high oxygen impurity amount.

Second test experiments are performed with two test cases that have different operating pressures and oxygen impurity amounts while other parameters are fixed. In this comparison two discharges with different electron temperatures expected. Difference in measured electron temperature is observed as expected.

However, transmitted emissions with 2.3 μm thickness aluminum foil are too low compared with 0.8 μm and 1.5 μm thickness aluminum foil. With this result measured electron temperature is below 20 eV. There is large difference in two test experiments. Low transmitted emission level of 2.3 μm can be explained by assuming the presence of non-thermal high energy radiations. And combined effect of non-thermal high energy radiation and oxygen impurity line radiation can be explaining the difference in measured electron temperature. When more precise diagnostics for these radiations is prepared, the potion of these radiation compare with continuum radiation can be determined then it is possible to diagnose the electron temperature more precisely.

Keyword: Soft X-ray absorber foil method, Two foil technique, electron temperature, Soft X-ray, VEST, AXUV

Student Number: 2012-21012

Contents

List of Figures

Chapter 1 Introduction

Because of the harsh conditions in high temperature plasma it is hard to diagnose the plasma status. However without precise information about the plasma it is hard to progress further experiment. So diagnostics for plasma is very important for plasma control and physics evaluation. [1].

In VEST for the edge region plasmas there are two triple Langmuir probes in upper and main chamber. So we can measure the evolution of electron temperature and electron density in edge region plasmas. However it is impossible to use these probes in the core region plasmas because of the thermal damage. In this reason optical diagnostics are necessary for core region plasmas. Thomson scattering system is under development for the precise measurements of electron temperature and density. However there are two problems. First, it takes too long time to development. Second, in the initial phase because of the laser pulse interval time only one temporal point is available, that is to say impossible to see the evolution of electron temperature and density in a single discharge so complementary diagnostics are necessary. For the electron density there is 94GHz interferometer is developed. With the tomography method like Abel inversion it is possible to get the radial electron density profiles. However there is no substitute and supplement diagnostics for electron temperature. SXR absorber foil method [2] is relatively simple electron temperature diagnostic method with good time and spatial resolution. Largely there are four features on this method. First, this method is simple to realize compare with other optical electron temperature diagnostics like

Thomson scattering. Second, this method has good time and spatial resolution. Usually multi-element photodiode is used as a detector and the time and spatial resolution can be about 500ns and few centimeter order. So evolution of electron temperature can be measure. Third, with the tomography method it gives two dimensional electron temperature profiles [3]. Fourth, this is passive method so it doesn't perturb the plasma.

SXR absorber foil method is application of SXR diagnostics. [4] Soft X-ray diagnostics is usually categorized in three with respect to the energy resolutions. First, high energy resolution, X-ray crystal spectroscopy. This diagnostics primarily used to determine ion temperature and flow velocity. Second, moderate energy resolution, pulse height analysis spectrometer. This method primarily used to determine concentration of impurities in the plasma. Third, crude resolution, absorber foils with SXR photodiode, it's one dimensional SXR cameras. With the several SXR cameras could measure the emission profiles of SXR. This profile is useful for identifying plasma MHD behaviors. SXR absorber foil method is application of this one dimensional SXR camera.

SXR absorber foil method use two one dimensional SXR cameras which have same line of sight. In front of each camera there is optical filter with different thickness. Usually thin metal foil is used for this purpose. So low energy photons are blocked and high energy photons transmit the filters. Because of the difference in transmission rate in two different thickness foils there is difference in transmitted photons and also signals in SXR cameras. In most cases the ratio between two signals is function of electron temperature

only and it can be used as an electron temperature diagnostic tool. The next chapter is about theoretical approach to how the ratio could be a function of electron temperature only and necessary condition for this method.

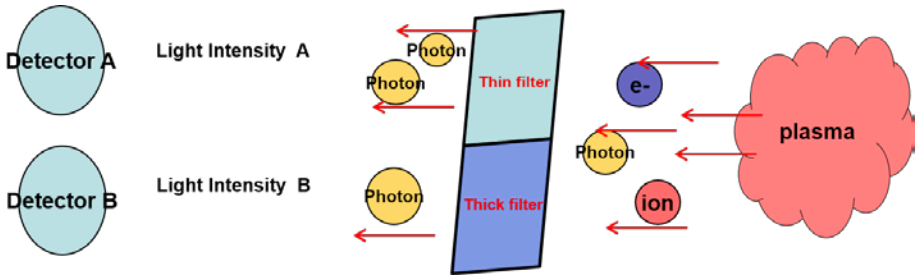

Figure 1.1 Schematic diagram of Soft X-ray absorber foil method

Chapter 2 Theoretical background

2.1 Radiation mechanisms of Soft X-ray in fusion device

Because this diagnostics focused on SXR it is important to know the mechanisms of this radiation. The source of photon energy is come from the energy difference of initial and final energy state of electrons. It can be categorized in three with respect to the initial and final state. [5]

First, free-free radiation, also called bremsstrahlung radiation which means braking radiation. Free-free means the initial and final state of electrons is free state. For this reason this spectrum is continuum. It is emitted by changes in free electron velocity by Coulomb field generated by charged particles.

Second, free-bound radiation, also called recombination radiation. Its mechanism is similar with bremsstrahlung radiation but the final state of free electron is bound state. For this reason it is called free-bound radiation. This mechanism produces also continuum radiation.

The last mechanism is bound-bound radiation which is same with characteristic line radiation. This is produced by transitions of bound electrons from high state to low state. Because the initial and final states are bound it is called bound-bound radiation.

These three mechanisms are important in SXR absorber foil method in different aspect. SXR is optically thin in plasma hence no need to consider reabsorption or photo-ionization. In this chapter, brief description will be presented for the detail descriptions following references are helpful. [6,7]

In next section the relationship between SXR absorber foil method and

each mechanism is discussed.

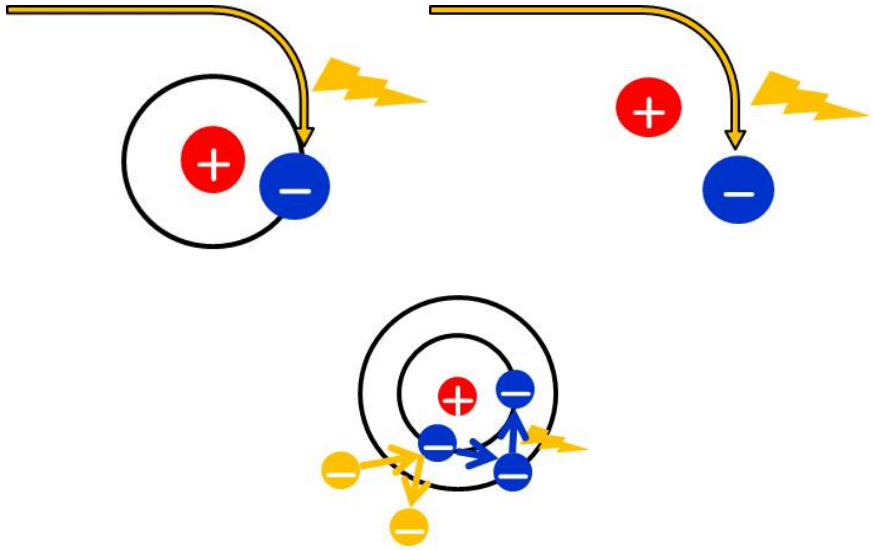

Figure 2.1 schematic diagram of bremsstrahlung, recombination and characteristic line radiation

2.2 Soft X-ray absorber foil method

In conventional fusion device bremsstrahlung radiation is major mechanism for SXR because of the high electron temperature the fraction of recombination radiation and line radiation is relatively small. However in the small device like VEST recombination radiation and line radiation is also abundant due to the relatively low electron temperature. In this chapter the feasibility of soft X-ray absorber foil method in terms of bremsstrahlung radiation, recombination radiation and characteristic line radiation is

considered.

2.2.1 Continuum radiation and soft X-ray absorber foil method.

Bremsstrahlung radiation and recombination radiation has similar form both are function of plasma density, electron temperature and impurities. In this chapter the emission power spectrum for bremsstrahlung and recombination radiation is derived and it is proved that SXR absorber foil method is well applicable in continuum radiation.

First, bremsstrahlung radiation emission power spectrum is described as follow. [8]

$$\left(\frac{\mathrm{dW}}{\mathrm{d}h\upsilon}\right)_{\mathrm{ff}} = \frac{32}{3\sqrt{3}}\left(\frac{\pi}{2}\right)^{\frac{1}{2}}\left(\frac{e^2}{\hbar c}\right)^3 \frac{\hbar^2}{m^{3/2}}\mathrm{n_e}\left(\sum_i n_i Z_i^2\right)\frac{\exp(-h\upsilon/T_e)}{T_e^{1/2}}\overline{g_{ff(T_e,h\upsilon)}} \tag{2.1}$$

or

$$\left(\frac{\mathrm{dW}}{\mathrm{d}h\upsilon}\right)_{\mathrm{ff}} = 3\times 10^{-15}\mathrm{n_e}\left(\sum_i n_i Z_i^2\right)\frac{\exp(-h\upsilon/T_e)}{T_e^{1/2}}\overline{g_{ff(T_e,h\upsilon)}}\ \mathrm{cm^{-3}}\ s^{-1} \tag{2.2}$$

where T_e is expressed in keV and $\overline{g_{ff(T_e,\mathrm{h}\upsilon)}}$ which is the Gaunt factor averaged over a Maxwellian distribution.

This can be derived from nonrelativistic Sommerfeld expression for the

angle integrated cross section which assumes isotropic electron distribution function and nonrelativistic case.

$$\sigma(\mathrm{h}\upsilon) = \frac{16}{3}\frac{\pi}{\sqrt{3}}\left(\frac{e^2}{\hbar \mathrm{c}}\right)^3 Z^2 \frac{\hbar^2}{2m\epsilon}\frac{g_{ff(\epsilon,\mathrm{h}\upsilon)}}{\mathrm{h}\upsilon} \tag{2.3}$$

where ϵ is the incident electron energy, $\mathrm{h}\upsilon$ the emitted photon energy. The Gaunt factor $g_{ff(\epsilon,\mathrm{h}\upsilon)}$ has been derived by Sommerfeld in a wide range of ϵ and $\mathrm{h}\upsilon$.

From this cross section the expression for the emission power spectrum can be deduced.

$$\left(\frac{\mathrm{dW}}{\mathrm{d}h\upsilon}\right)_{\mathrm{ff}} = \frac{16}{3}\frac{\pi}{\sqrt{3}}\left(\frac{e^2}{\hbar \mathrm{c}}\right)^3 \left(\sum_i n_i Z_i^2\right)\frac{\hbar^2}{m^{3/2}}\int_{h\upsilon}^{\infty}\frac{g_{ff(\epsilon,h\upsilon)}f(\epsilon)}{\sqrt{2\epsilon}}\mathrm{d}\epsilon \tag{2.4}$$

where n_z is the ion density of effective charge Z and $f(\epsilon)$ is electron distribution function. It is possible to assume that electrons are at the thermal equilibrium due to the high mobility so $f(\epsilon)$ is a Maxwellian function.

$$f(\epsilon) = \frac{2n_e\epsilon^{1/2}}{\pi^{1/2}{T_e}^{3/2}}\ \exp(-\epsilon/\mathrm{T_e}) \tag{2.5}$$

Equation (2.2) can be deduced from equation (2.4) and (2.5).

Second, recombination radiation is emitted by free electrons captured in a hydrogen or impurity ion which energy is summation of initial electron kinetic energy 'ϵ' and binding energy of the recombination level 'χ_n'.

$$h\upsilon = \epsilon + \chi_{\mathrm{n}} \tag{2.6}$$

Radiative recombination cross section of hydrogen-like ions is like below.

$$\sigma_{\mathrm{r}}(\epsilon, n, Z) = \frac{8\pi}{e\sqrt{3}}\frac{Z^2e^6}{\hbar \mathrm{c}^3 m}\frac{\chi(Z,n)}{\epsilon}\frac{g(n)}{n^3}\frac{g_{fb}(\epsilon,n,Z)}{h\upsilon} \tag{2.7}$$

where

$$\chi(Z,n) = \frac{\chi_{\mathrm{H}} Z^2}{n^2} = \frac{13.6Z^2}{n^2}\ (eV) \tag{2.8}$$

$$\mathrm{g(n)} = 2\mathrm{n}^2 \tag{2.9}$$

g(n) is the statistical weight of the recombined level and $g_{fb}(\epsilon, n, Z)$ free-bound radiation gaunt factor. Equation (2.7) can be deduced from the photoionization cross section of hydrogen-like ions which is better studied. With some approximations for the other types of ions and use Maxwellian function for electron distribution the emission power spectrum of recombination radiation is given by [8]

$$\left(\frac{\mathrm{dW}}{\mathrm{d}h\upsilon}\right)_{fb} = 3\times 10^{-15} n_e \frac{exp(-h\upsilon/\mathrm{T_e})}{T_e^{1/2}} \times \left\{ \sum_i n_{\mathrm{i}} Z_i^2 \left[G_n \frac{\xi}{n^3} \frac{\chi_{\mathrm{i}}}{T_e} \exp(\chi_{\mathrm{i}}/T_e) + \sum_{m>n} G_m \frac{2\chi_{\mathrm{H}} Z_i^2}{T_e m^3} exp\left(\frac{Z_i \chi_{\mathrm{H}}}{T_e m^3}\right) \right] \right\} \tag{2.10}$$

where n is the principal quantum number of the fundamental shell, $\mathrm{n_z}$ is impurity density of nuclear charge Z and G_n and G_m are averaged Gaunt factor which calculated for hydrogenic ions by Karzas and Latter.[9,10] These Gaunt factors have been assumed equal to unity due to negligible variation in interesting region.

Bremsstrahlung radiation and recombination radiation has similar form of emission power spectrum so it can be combined with one formula.

$$\left(\frac{\mathrm{dW}}{\mathrm{d}h\upsilon}\right)_{ff+fb} = 3\times 10^{-15} n_e^2 Z_{eff} \frac{exp\left(-\frac{h\upsilon}{\mathrm{T_e}}\right)}{T_e^{1/2}} \times G \tag{2.11}$$

$$Z_{eff} = \sum_i \frac{n_i Z_i^2}{n_e} \tag{2.12}$$

$$G = \overline{g_{ff}} + G_n \frac{\xi}{n^3} \frac{\chi_i}{T_e} \exp\left(\chi_i / T_e\right) + \sum_{m>n} G_m \frac{2\chi_H Z_i^2}{T_e m^3} exp\left(\frac{Z_i \chi_H}{T_e m^3}\right) \tag{2.13}$$

The free-free and free-bound Gaunt factors can be assume unity thus G is independent of photon energy.

As described above the emission power spectrum of continuum radiation is function of electron density, electron temperature and Z effective. And if there is a metal foil this radiation is absorbed according to filter materials and thickness.

$$P_{filtered} = \int \frac{\mathrm{dW_{ff+fb}}}{\mathrm{d}h\upsilon} \mathrm{T(E)}\ dE \tag{2.14}$$

T(E) is transmission function of metal foil. In the thick foil large absorption occurred and in the thin foil small absorption occurred so there is intensity difference between two transmitted radiations.

$$P_{thin} = \int \frac{\mathrm{dW_{ff+fb}}}{\mathrm{d}h\upsilon} \mathrm{T}_{thin}\mathrm{(E)}\ dE \tag{2.15}$$

$$P_{thick} = \int \frac{\mathrm{dW_{ff+fb}}}{\mathrm{d}h\upsilon} \mathrm{T_{thick}(E)}\ dE \tag{2.16}$$

The ratio of this two filtered power is given by

$$\mathrm{Ratio(T_e)} = \frac{P_{thin}}{P_{thick}}$$

$$= \frac{\int_{E_{cut}}^{\infty} 3 \times 10^{-15} n_e^2 Z_{eff} \frac{exp\left(-\frac{h\upsilon}{\mathrm{T_e}}\right)}{T_e^{1/2}} \times G \times \mathrm{T}_{thin}\mathrm{(E)\,dE}}{\int_{E_{cut}}^{\infty} 3 \times 10^{-15} n_e^2 Z_{eff} \frac{exp\left(-\frac{h\upsilon}{\mathrm{T_e}}\right)}{T_e^{1/2}} \times G \times \mathrm{T}_{thick}\mathrm{(E)\,dE}} \tag{2.17}$$

$$= \frac{3 \times 10^{-15} n_e^2 Z_{eff} T_e^{-1/2} \times G \int_{E_{cut}}^{\infty} exp\left(-\frac{h\upsilon}{\mathrm{T_e}}\right) \times \mathrm{T}_{thin}(\mathrm{E})\,\mathrm{dE}}{3 \times 10^{-15} n_e^2 Z_{eff} T_e^{-1/2} \times G \int_{E_{cut}}^{\infty} exp\left(-\frac{h\upsilon}{\mathrm{T_e}}\right) \times \mathrm{T}_{thick}(\mathrm{E})\,\mathrm{dE}}$$

$$= \frac{\int_{E_{cut}}^{\infty} \frac{exp\left(-\frac{h\upsilon}{\mathrm{T_e}}\right)}{T_e^{1/2}} \times \mathrm{T}_{thin}(\mathrm{E})\,\mathrm{dE}}{\int_{E_{cut}}^{\infty} \frac{exp\left(-\frac{h\upsilon}{\mathrm{T_e}}\right)}{T_e^{1/2}} \times \mathrm{T}_{thick}(\mathrm{E})\,\mathrm{dE}}$$

The photon energy dependent term is exponential term and foil transmission term so the other terms are come out from the energy integral. For this reason the ratio of two transmitted power is function of electron temperature only. So for the continuum radiation there is no problem to use SXR absorber foil method as an electron temperature diagnostic tool.

2.2.2 Characteristic line radiation and soft X-ray absorber foil method

If there is line radiation which available to penetrate the foil the total radiation power will be changes.

$$\mathrm{Ratio} = \frac{P_{thin}}{P_{thick}}$$

$$= \frac{\int \left(\frac{\mathrm{dW_{ff+fb}}}{\mathrm{d}h\upsilon}\right) \mathrm{T}_{thin}(\mathrm{E})\ dE + line \times\ \mathrm{T}_{thin}(\mathrm{E})}{\int \frac{\mathrm{dW_{ff+fb}}}{\mathrm{d}h\upsilon}\ \mathrm{T}_{thick}(\mathrm{E})\ dE + line\ \times\ \mathrm{T}_{thick}(\mathrm{E})}$$

$$= \frac{\int_{E_{cut}}^{\infty} exp\left(-\frac{h\upsilon}{\mathrm{T_e}}\right) \times \mathrm{T}_{thin}(\mathrm{E})\,\mathrm{dE} + \frac{line \times \mathrm{T}_{thin}(\mathrm{E})}{3 \times 10^{-15} n_e^2 Z_{eff} T_e^{-1/2} \times G}}{\int_{E_{cut}}^{\infty} exp\left(-\frac{h\upsilon}{\mathrm{T_e}}\right) \times \mathrm{T}_{thick}(\mathrm{E})\,\mathrm{dE} + \frac{line \times \mathrm{T}_{thick}(\mathrm{E})}{3 \times 10^{-15} n_e^2 Z_{eff} T_e^{-1/2} \times G}} \quad (2.15)$$

$$line^{*} = \frac{line}{3 \times 10^{-15} n_e^2 Z_{eff} T_e^{-1/2} \times G} \quad (2.16)$$

Transmitted characteristic line radiation has different form with continuum

radiation so the ratio is not function of electron temperature only. In this situation one to one correspondence between intensity ratio and electron temperature is impossible because of density and impurity term is not erased. However by assuming the amount of eq. (2.16) the effect of line radiation is can be identify. Furthermore if line radiation emission spectrum is given through the experimental data it is also possible to use electron temperature diagnostic tools, of course electron density, temperature and Z effective are given or estimated.

To identify the line radiation effect calculations are performed with the assumption of the quantity of eq. (2.16). In here Gaunt factor is also assumed unity. In low energy region which range is below 80 eV and high energy region which range is between 300 eV to 400 eV various intensity is considered. It is assumed that the amount of eq. (2.16) is 10, 100, 1000 and 10000 % of exponential term in continuum radiation. Figure 2.2 and 2.3 are these result. The effect of low energy lines are the intensity ratio and electron temperature plot is lower shifted by line emission amount increase. So below 90 eV of electron temperature it could overestimate the experimental result. The effect of high energy lines is that the intensity ratio and electron temperature plot is upper shifted by high energy line emission amount increase. So as seen in the figure 2.3 the experimental result could be under estimated.

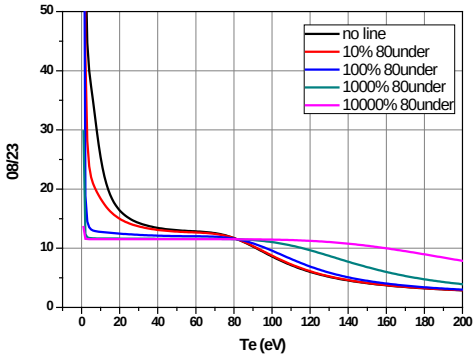

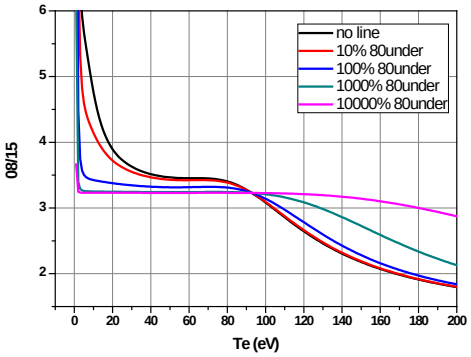

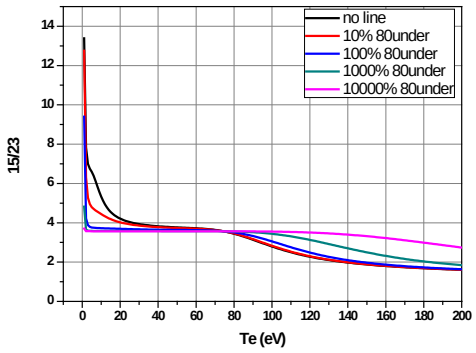

Figure 2.2 oxygen line radiation effect

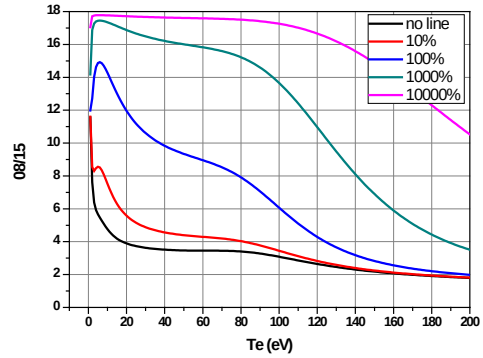

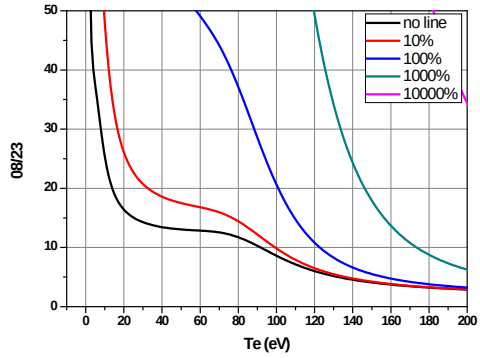

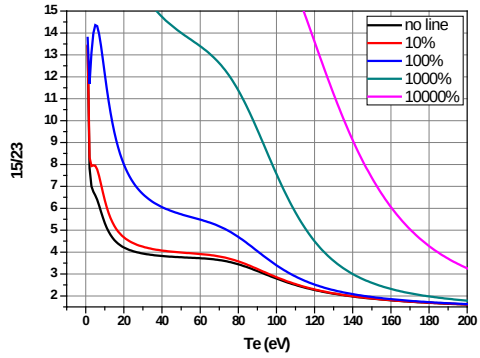

Figure 2.3 300~400 eV range non-thermal high energy photon effect

As described in above figures without the line radiation information it has uncertainties in measurements hence estimate the possible transmitted line radiation is important. However if the amount of impurity not much changes in time relative value of electron temperature is still useful.

Chapter 3 Overall system design

3.1 Filter material and thickness

3.1.1 filter materials

Expected electron temperature in the VEST core region plasma is about 100 eV. Because it is relatively low values so the continuum radiation emission power at high energy photon region will be low. (fig. 3.1) For this reason there are two requirements for filter materials. First, the transmission rate in the low photon energy region below the 1keV should be high. For the high signal strength it is important to use appropriate filter that has good transmission rate in the low photon energy region. Second, it should have proper cut off energy in transmission rate. If the transmission rate cut off energy is too low the abundant hydrogen characteristic line radiation can affect to the detector. As mentioned last chapter it can be act as an error source thus at least the filter have to has higher cut off energy than hydrogen characteristic line radiation that is 13.6 eV. To meet these purposes low Z metals are suitable. Aluminum is chosen due to its high transmission rate in low energy photon region and the easy procurement.

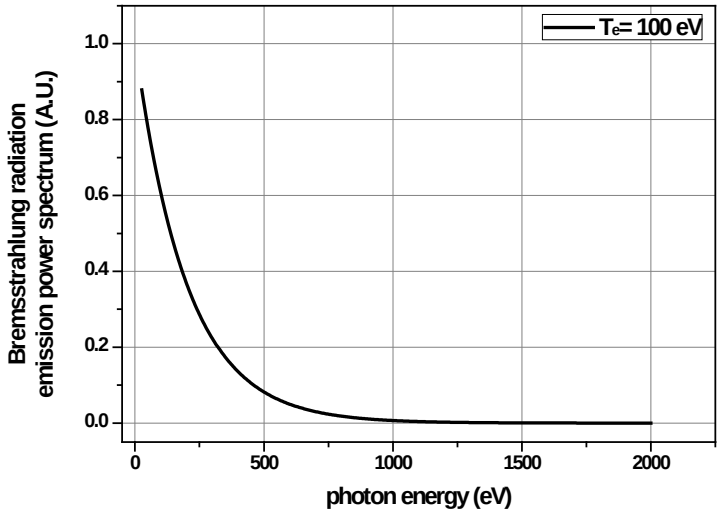

Figure 3.1 Bremsstrahlung radiation emission power spectrum

3.1.2. Filter thickness

Measureable range of electron temperature is determined by thickness combination of metal foil. So it is important to choose appropriate thickness combination.

Calculations for the relationship between electron temperature and intensity ratio have been performed for determination of foil thickness combination on the basis of transmission rate database [11]. When increase thickness difference between two foils the measurable range is move to the higher electron temperature region and when increase both filter thickness with same thickness difference the measurable range is move to the lower electron temperature region. On the basis of these result 0.8 μm and 1.5 μm aluminum foil combination has been chosen due to appropriate for measure around 100 eV electron temperatures and has relatively high signal strength.

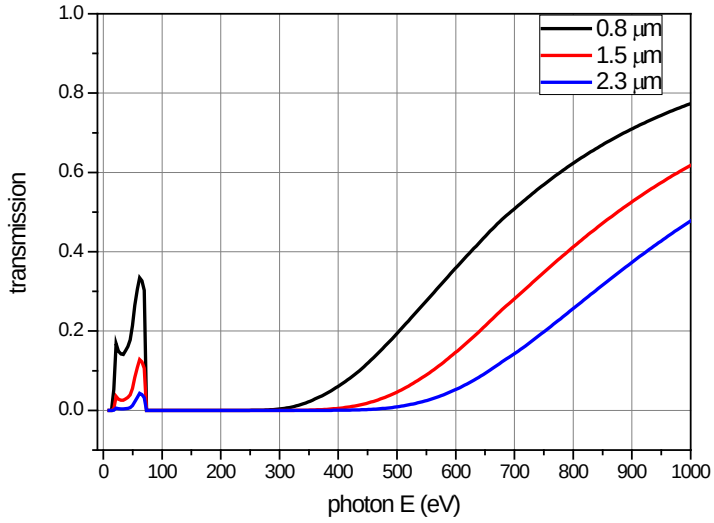

Figure 3.2 Transmission rate of aluminum foil with thickness of 0.8 μm, 1.5 μm and 2.3 μm

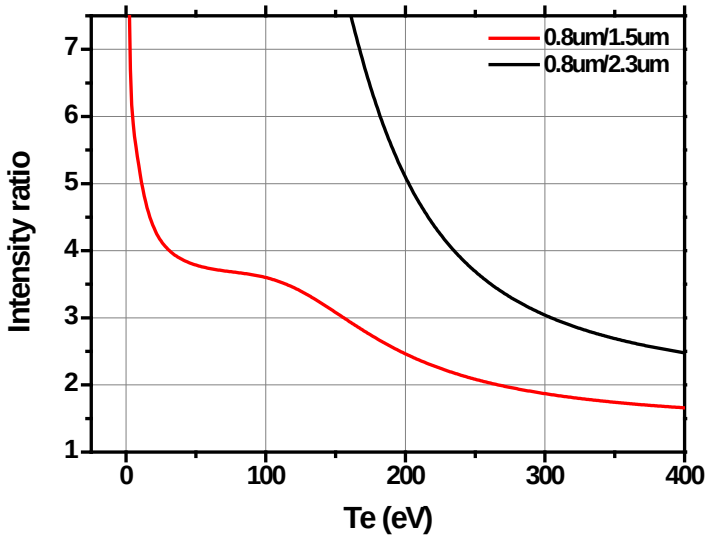

Figure 3.3 Intensity ratio between power filtered by 0.8 μm and 1.5 μm and 0.8 μm and 2.3 μm

However there is some problem in this foil combination. In VEST the expected major impurity is oxygen. Because tungsten limiter is used instead of graphite limiter thus carbon impurity will be relatively small. And because of the relatively low plasma temperature the expected metal impurity rates is also small. In this reason the expected major impurity is oxygen from the water vapor in vacuum chamber. Below the 100eV photon energy region there are characteristic lines of oxygen that possible to transmit this thickness combination. [12] So as described in chapter 2 some uncertainties are expected in measured electron temperature. However by choosing appropriate detectors which more sensitivity on the high energy photon region this effect will be reduced. Details are discussed in the next section.

3.2Detector

AXUV-16ELG photodiode is chosen as a detector. AXUV means Absolute eXtreme Ultra Violet. The main feature of this photodiode is that it can detect SXR region photon directly that is no need to additional scintillator. It consists of 16 detector elements of photodiode. Each single photodiode has 2 mm × 5 mm active area and its gap distance between nearby elements is 0.12 mm (fig. 3.3). From this relatively small size it can be used as high spatial resolution SXR camera. And also it has good time response. Its nominal rise time is 500 nsec so many fast events are detectable [5, 13, 14]. Another remarkable feature of this photodiode is that it has good and almost linear quantum efficiency in ultra violet to soft X-ray region

photons (fig.3.4). From this feature the higher photons generates the more charge carriers in photodiode thus the information of incident photons remains as electrical signal. In other words it acts as weighting factor on high photon energy region. Because expected major impurity is oxygen it is possible to assume that high photon energy region (above 200 eV) is free from impurity characteristic lines. For this reason the impurity characteristic line emission effect is relatively reduced.

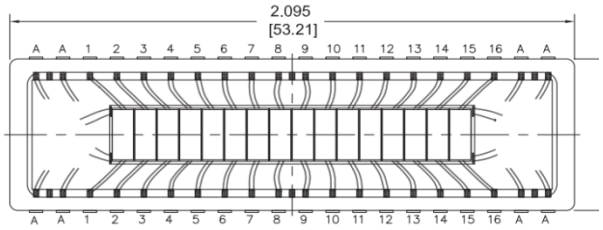

Figure 3.4 AXUV 16 ELG [14]

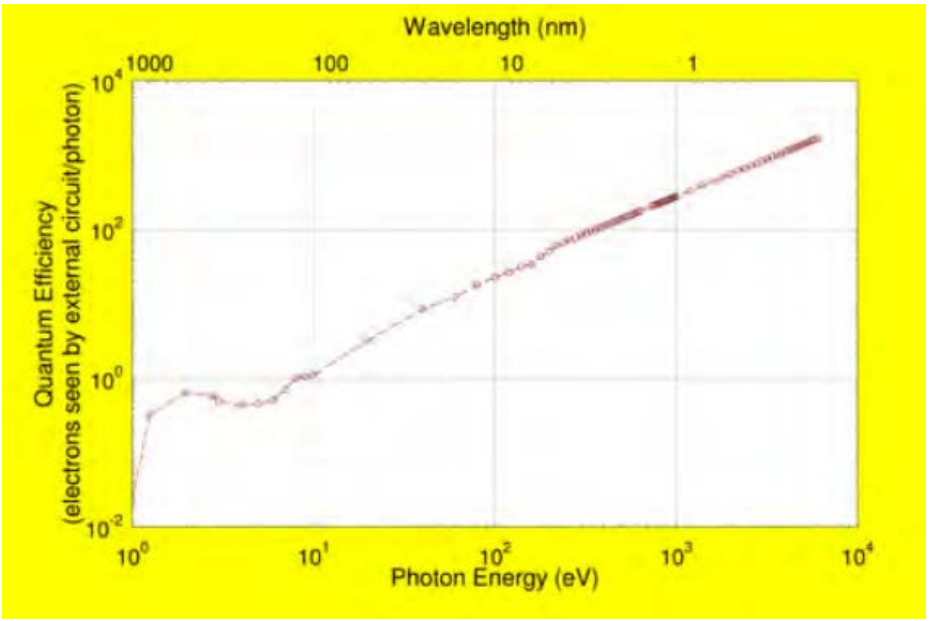

Figure 3.5 Quantum efficiency of AXUV 16ELG [14]

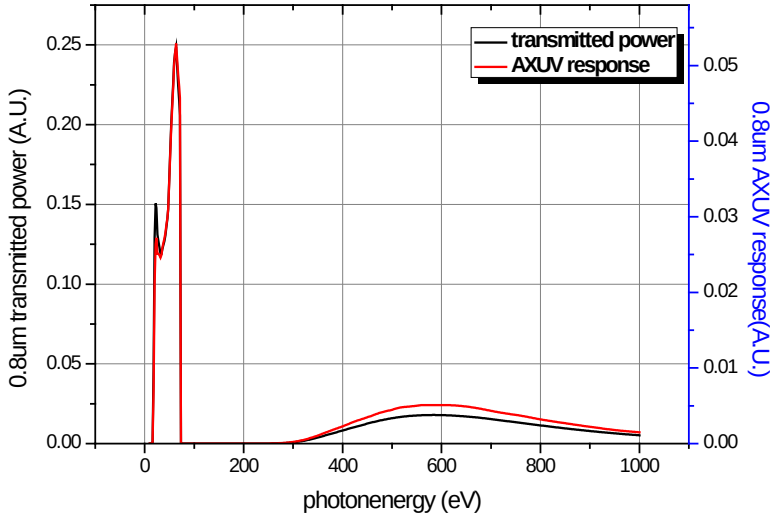

Figure 3.6 transmitted power and AXUV response

3.3. Amplifier

Inverse amplifying circuit is used due to the low raw signal level. Low noise, high gain and wide bandwidth frequency are requirements of appropriate amplifier. Because the AXUV photodiode has 0.5 μs rising time, generally it is amplifier that limits the maximum bandwidth of detection. In this purpose OP484 operational amplifier which produced by Analog Devices is chosen. Nominally it has 4 MHz bandwidth and in experimentally negligible gain drops within 100 kHz [15]. Thus it can be used for wide range of phenomena detection. Furthermore it has rail to rail inputs and outputs which guarantees that signal amplification to the maximum power of biased power. With this operational amplifier the 100 kΩ resistor is connected between the input and the output and there is 1 kΩ in front of input terminals. Voltage gain of this amplifier is 100.

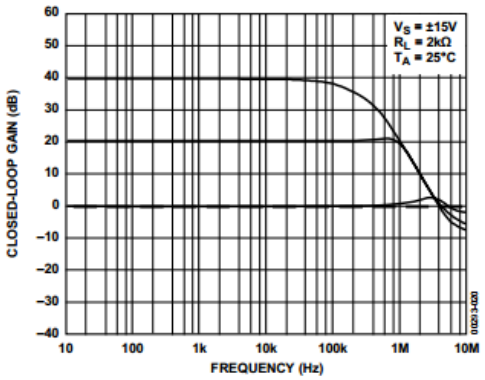

Figure 3.7 OP484 closed loop gain

3.4 Assembly of diagnostic system and installation on VEST

3.4.1 foil and detector holder

It is too common to mention that reject the unwanted light is important however it is important especially in visible light region. Due to not only high reflexibility of visible light but also the high intensity and high sensitivity of AXUV photodiode on that region even if small leak it can be large affect. So the surface of diagnostic system assembly is coated with black and by overlapping each other eliminates the light leak. Block the filter hole with 105 μm aluminum foil which originally for the 1.5 μm and 0.8 μm aluminum foils. 105 μm has high cutoff energy about 5 keV so in VEST condition it is possible to assume that no photons can transmit this thick foil. Visible light leak experiments conducted in maximum visible light intensity condition plasmas in VEST which is ECH pre-ionized ohmic plasma its current is about 60kA. With the test experiments there is no response in detectors so no visible light effect in VEST plasma conditions on detector.

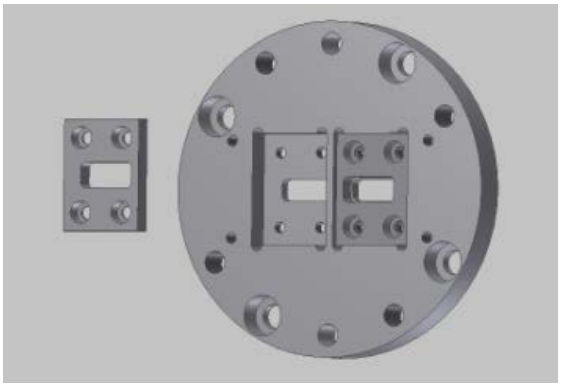

Figure 3.8 foil and detector holder

3.4.2 Detector position

This diagnostic system is located on mid-plane of VEST chamber to diagnose core region plasma [figure 3.11]. Unlike with other fusion device like Stellarator it is possible to assume toroidal symmetry in Tokamak. Due to this property toroidally separated two detectors sees same plasma although they are not in same position. If the two toroidally separated distance is small compare with size of VEST this assumption is well applicable.

AXUV photodiode is arranged in toroidal direction hence it is possible to apply torodidal symmetry property. Since this photodiode has 16 channels two of them is selected which distance between two channels is 17 mm. It is 8.7×10^{-3} radians from the center of the VEST chamber.

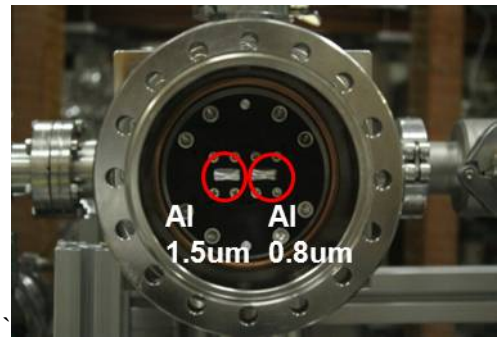

Figure 3.9 Filter foil holder

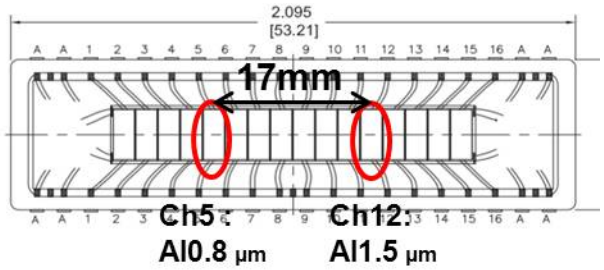

Figure 3.10 used channels of photodiode

Figure 3.11 Picture of whole system (in the red circle)

3.4.3 Collimator

Without the optical component like pinhole or collimator the spatial information about the source plasma is too vague. Actually the small line of sight gives more precise diagnostic result however because of the low expected soft X-ray signals firstly large line of sight is determined. 1m length stainless steel pipe is used as a collimator. With this collimator the diameter of sight cone at the core plasma region is reduced to 128 mm. There is also slot for collimator in front of the foil holder. When the signal level is determined more precise collimator will be used.

3.4.4 Electromagnetic interference consideration

Signal lines from detector are transferred to the signal processing circuit via electrical vacuum feedthrough. However because of the high electrical power and high electromagnetic filed circumstance in fusion device there are electromagnetic interference (EMI) based on largely two coupling mechanisms which are conductive coupling and free-space coupling.

First, conductive coupling EMI occurs when there is conductor path between two circuits. The main source of conductive coupling mechanism is power ground path. To remove this path and also conductive coupling noise source battery power based DC-DC convertor is used. Additionally from this stable power supply is available. Due to the imperfect rectification AC power based AC-DC convertor is unchosen. Second, available free-space

coupling EMI is inductively coupled (near field) and radiative coupled (far field) EMI. Inductively coupled noise is from inductive pick up in the loop of signal lines. It can be reduced by twist the signal lines and removes the area of loop. In this reason each signal lines are twisted. In VEST 2.45 GHz microwave is used for preionization. This microwave can cause radiative coupled noise. By appropriately shielding the signal lines this type of interference can be reduced. The signal lines are covered with copper braided wire in this purpose. Since the copper braided wire has 10 μm thick and smaller grid size compare with wavelength of the wave microwave cannot penetrate. [16, 17].

Chapter 4 Test experiments on VEST

4.1 Experimental setup

In addition to newly developed diagnostics three other diagnostics are used for interpretation of the test experiment data. There are two photodiode for monitoring H-alpha line and oxygen characteristic line and one triple Langmuir probe for monitoring electron density and temperature of edge plasmas.

H-alpha is characteristic line radiation of hydrogen atom whose wave length is 656.281 nm. Before the fully ionization state it may be assume that proportional to plasma density to some degree. As mentioned earlier oxygen is major impurity in VEST. Representative characteristic lines of oxygen atom exist around the wavelength of 777 nm furthermore in this region no characteristic lines of hydrogen. Thus this wavelength range may be used as representative of oxygen impurity amount. In these purpose 656 nm and 780 nm bandpass filters are chosen. (fig. 4.1 , fig. 4.2). DET10A/M photodiode is employed for detect these wavelength photons which has good responsivity 656 nm and 777 nm photons (fig. 4.3). Each photon signal is measured from outside of vacuum chamber via quartz window. There is negligible signal drops in quartz window because quartz has good and almost same transmission rate in these two wavelength range. Two bandpass filters are attached on the quartz window. These are located in the same horizontal plane with AXUV photodiode array and due to the toroidal symmetry it can be assumed that these three photodiodes sees same plasmas. In order to avoid electromagnetic noise photodiode stay away from the VEST chamber and the photon signals are transferred via optical fibers. It must be understood that these two diagnostics are not precise diagnostics for plasma density and oxygen impurity effect it gives just crude guidelines for plasma

density and oxygen impurity effect. Triple Langmuir probe is also used for the edge plasmas diagnostics which located in midplane of VEST chamber and radial scan is available. It may gives not only electron density and temperature absolute value of edge plasma but also impurity inflow information from the outboard which can be deduced from electron density and temperature evolution. With these three additional diagnostics test experiments are performed.

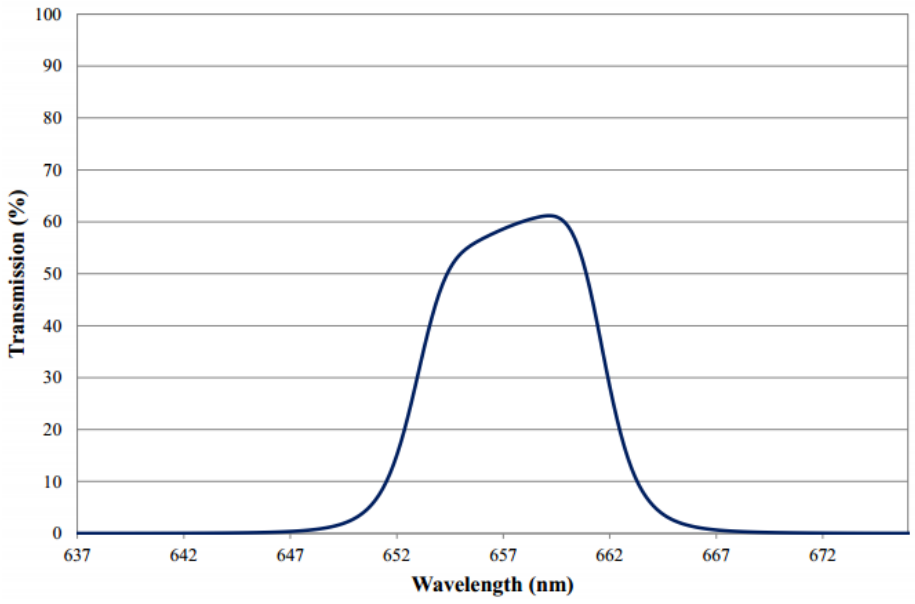

Figure 4.1 transmission curve of 656 nm bandpass filter [18]

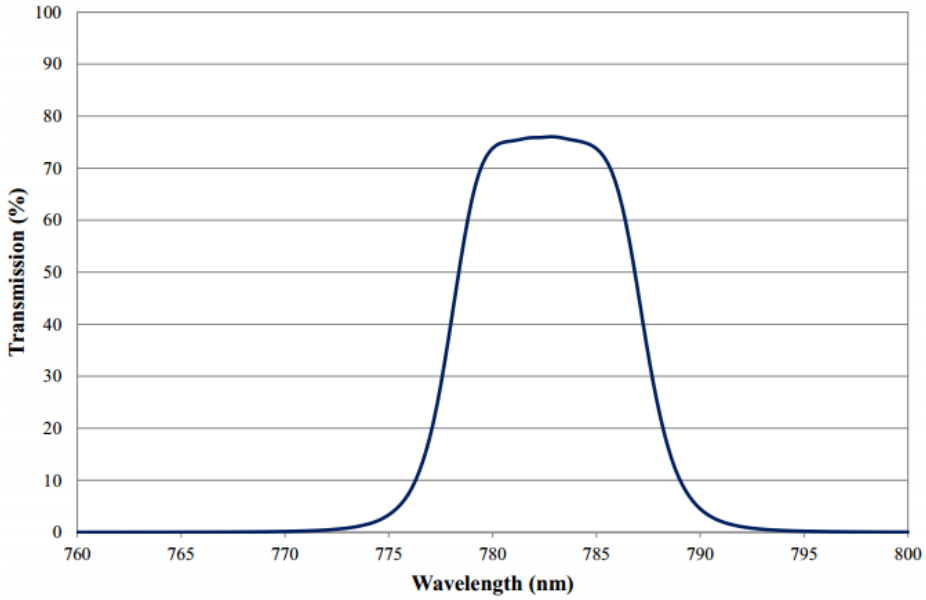

Figure 4.2transmission curve of 780 nm bandpass filter [18]

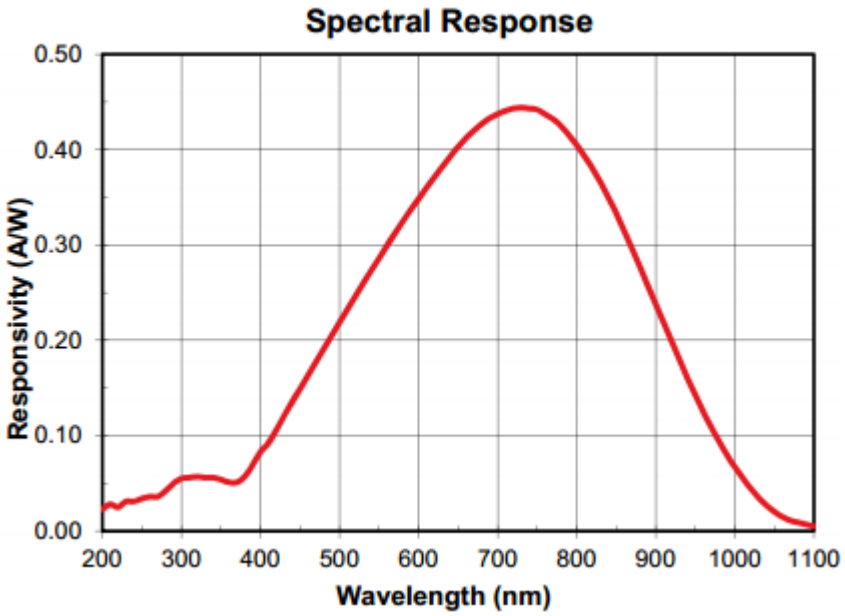

Figure 4.3 responsivity of DET10A/M [19]

4.2 Test experimental result

First experiment is performed with ECH preionized ohmic plasma as a target plasma. Its plasma current is about 60 kA and 10ms duration time. Its ohmic power is about 200kW and ECH 6kW heating constantly put into the plasma. The overall features of this discharge is like below figure (Fig. 4.4). Three line integrated signals have different tendency with plasma current. It continuously increases during the plasma current ramp down phase. In H-alpha signal because it is line integrated signal the edge region effect is also contained. Nonetheless increase in H-alpha even in current flattop region means that hydrogen gas is not fully ionized yet. So it is possible to use guide line for hydrogen ion density. Oxygen 777 nm line is also increases in whole discharge its possible source is vacuum chamber wall that is center stack and chamber outer wall. Even in plasma is separated with outer wall situation the oxygen 777nm line is increased from this it can be known that center stack and outer wall both are the oxygen impurity source.

From the ratio of two SXR signals electron temperature is obtained.(Fig.4.5) In order to minimize noise effect 1.5 μm foil signal is placed in denominator.

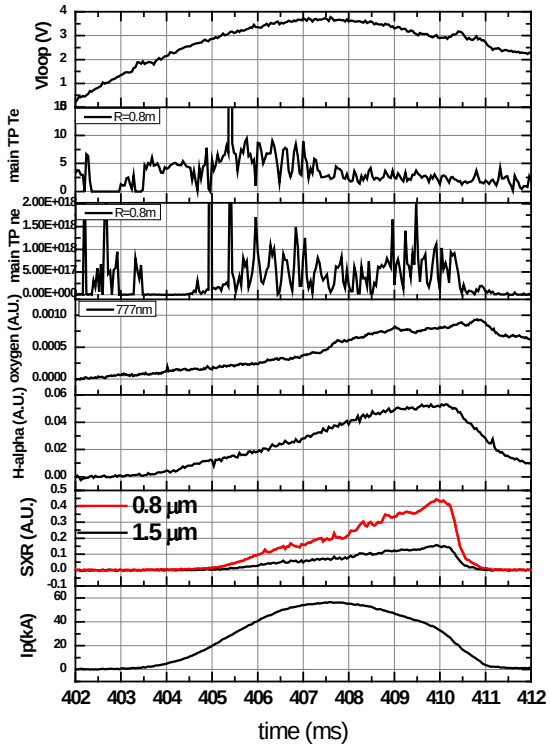

Figure 4.4 Test experiment shot #7029

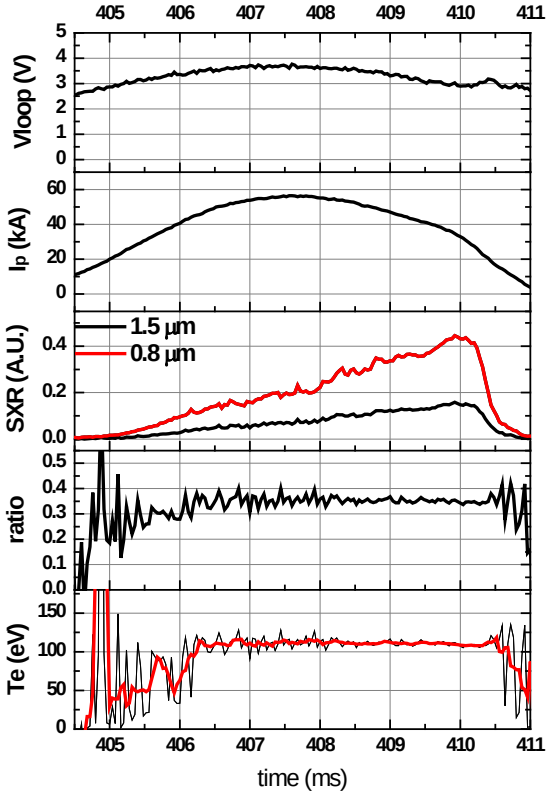

Figure 4.5 Measured electron temperature

Electron temperature at the maximum current region is about 110 eV. It's similar with expected value. Before the 405 ms there is large error due to the signal level of SXR is too low. Increase and decrease of the electron temperature is observed in before 406 ms and after 410.5 ms. There is constant electron temperature region from 406.3 ms to 410.5 ms. These results can be true. ECH power constantly put into the plasma and loop voltage is still high during this region. And also the plasma column size is decrease in this time so adiabatic compression effect is expected. So it can be sustained constantly. However also it can be false. As increase in oxygen 777 nm signals there is increase in inflow of impurities. Thus large uncertainty is expected.

Another experiment is performed with two test cases that have different operating pressures and oxygen impurity amounts while other parameters are fixed. This condition is produced by slightly changing poloidal magnetic field and decreasing operating pressure from #7181 discharge. #7182 discharge have lower operating pressure and lower oxygen impurity amounts compare with #7181 discharge in 405 to 408 ms. So in this region higher electron temperature of #7182 discharge is expected. The measured electron temperature is higher in #7182 discharge as expected.

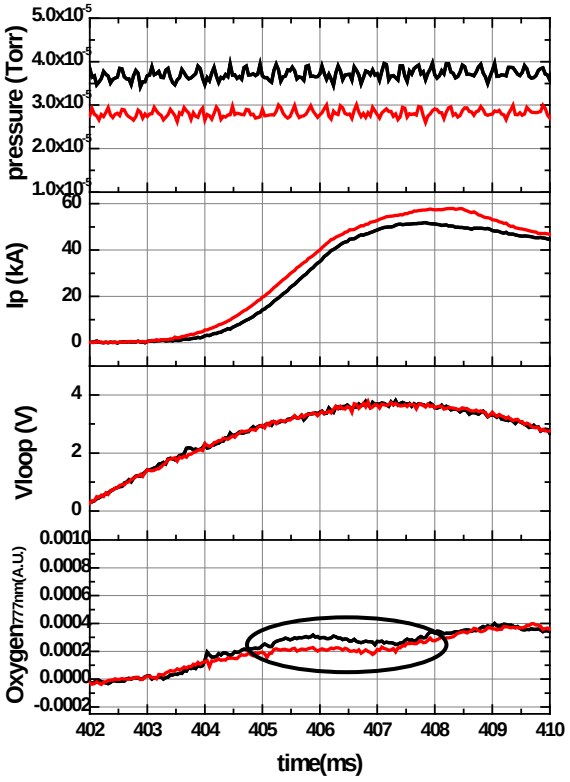

Figure 4.6 Second test experimental result.

Black line : shot #7181,

Redline : shot #7182

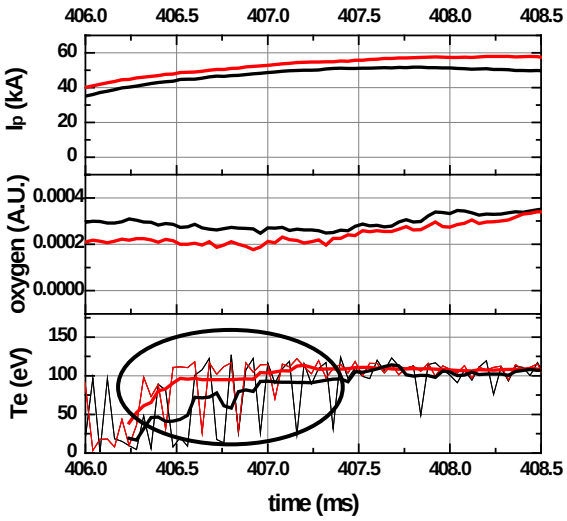

Figure 4.7 measured electron temperature

Black line : shot #7181,

Redline : shot #7182

To check previous two results 2.3 μm aluminum foil is used. Because the foil holder is optimized to use two foils shot by shot comparison is performed. [figure 4.8] Transmission difference with other thickness aluminum foil is like [figure 3.2]. Below 100 eV region and 300 eV to 500 eV regions have large difference in transmission rate. The measured ratio of 0.8 μm and 2.3 μm is about one-thirtieth to one-fortieth from the experimental data. [Figure 4.9] This value indicates about 10 to 20 eV. [Figure 4.10]. This is not coincidence with first test experimental data which value is about 110 eV. Furthermore it is impossible to explain this large signal difference between 0.8 μm and 2.3 μm from the oxygen line radiation effect. By assuming high energy non-thermal radiation this large difference can be explained. Moreover as mentioned in previous section if this non-thermal radiations exists there is underestimates in electron temperature. So it can be reducing the difference of two test experimental result.

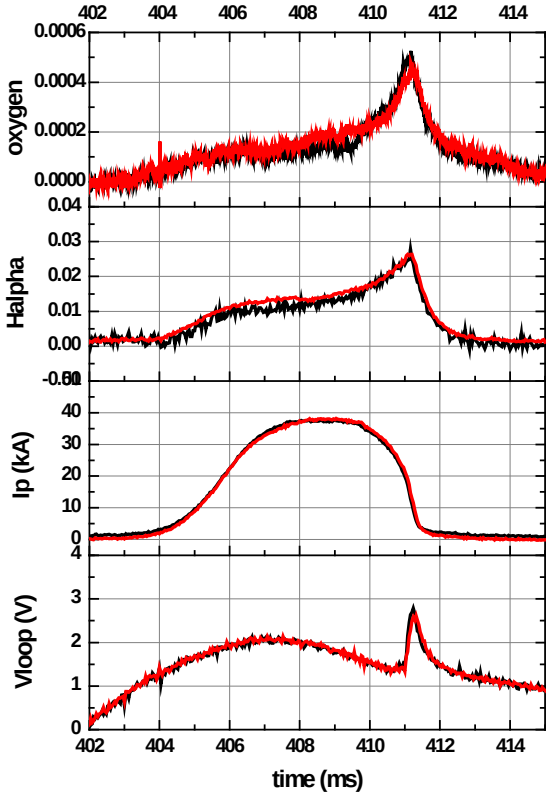

Figure 4.8 #7503 and #7517 discharge

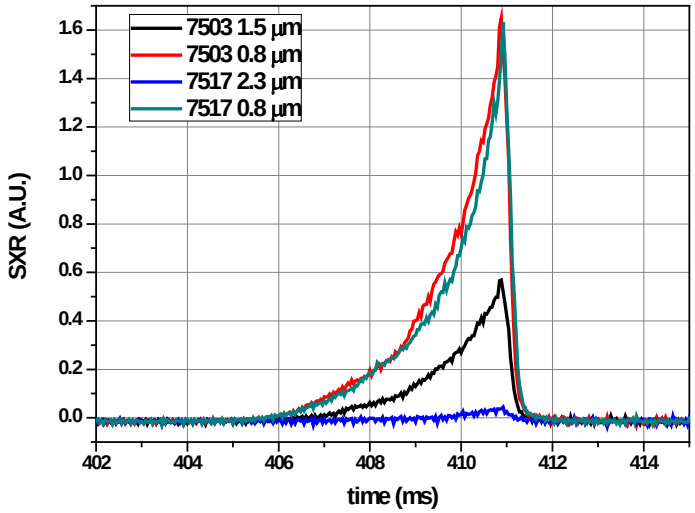

Figure 4.9 #7503 and #7517 discharge Soft X-ray signals

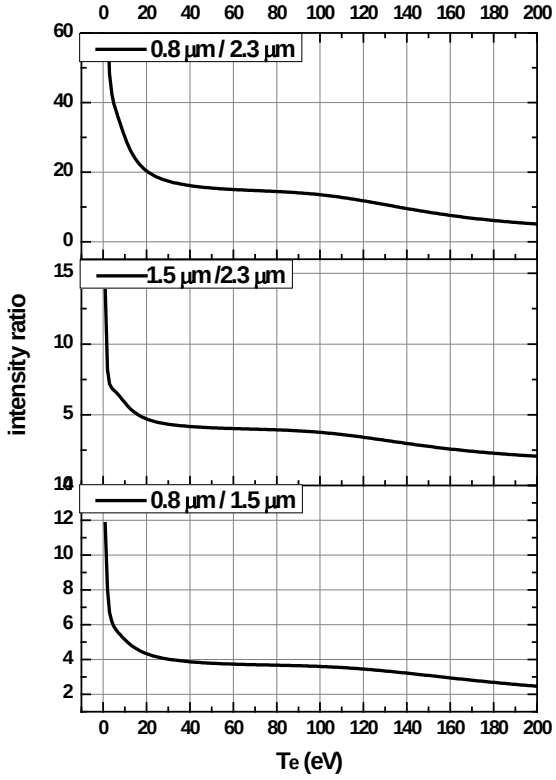

Figure 4.10 Intensity ratio versus electron temperature plot in three cases

Chapter 5 Conclusion and Future work

5.1Conclusion

Electron temperature diagnostics using SXR absorber foil method is successfully installed in VEST. From the first test experimental result electron temperature at the current peak region is about 110 eV. In the second test experiment measured electron temperature changes as expected. Thus this diagnostics identifies the change of electron temperature in some degree. However this value has uncertainties because of the expected oxygen ion characteristic line radiation and non-thermal high energy photons. This is identified or deduced from the oxygen atom 777 nm line radiation and 2.3 μm aluminum foil signal. In the below 100 eV electron temperature range, oxygen line radiation can be overestimates the electron temperature and non-thermal high energy photons underestimates electron temperature. By combining these two effects the experimental result can be matched.

5.2Future work

There is three kind of future work for increasing the reliability of developed diagnostics. First, minimize noise level. By doing this evolution of electron temperature at the current ramp up region can be more clearly observed. Second, change the design of foil holder in order that use four different thickness foils at the same time. In this case six different thickness combinations are possible so the cross check is possible each other. Third, install more precise diagnostics for impurity line radiation and non-thermal high energy photons. In this study impurity characteristic line radiation and non-thermal high energy photons are only qualitatively measured by crude diagnostics. In order to use SXR absorber foil method more reliably these two kind of radiation must be more precisely measured. For this purpose Pulse Height Analyzer is under consideration. When more precise diagnostics for these radiations is prepared, the portion of these radiation compare with continuum radiation can be determined then it is possible to diagnose the electron temperature more precisely.

Bibliography

[1] A.J.H. Donné et al., *diagnostics*, Nucl. Fusion, 47 S337 (2007)

[2] F. C. Jahoda et al., *Continuum radiation in the X ray and visible regions from a magnetically compressed plasma (Scylla)*, physical review, 3, 119 (1960)

[3] Seung Hun Lee et al., *Design and fabrication of a multi-purpose soft x-ray array diagnostic system for KSTAR*, Rev. Sci. Istrum. 83, 10E512 (2012)

[4] B.C. Stratton, *special issue on plasma diagnostics for magnetic fusion research, ch.5 passive spectroscopic diagnostics*, Fusion Science and Tech. Feb. (2008)

[5] J.H. Kim, *Analyses of the multi-step sawtooth crash behavior in the highly-elongated tokamak plasmas with the soft x-ray tomographic diagnostics*, Ph.D thesis, Korea Advanced Institute of Science and Technology

[6] I. H. Hutchinson, *Principle of Plasma Diagnostics*, (Cambridge university press, Cambridge,1987)

[7] G. Bekefi, *Radiation processes in plasmas*, (John Wiley & Sons, 1966)

[8] R. Bartiromo, *X-ray diagnostic of tokamak plasma*, Nucl. Istrum. and Meth. A255 (1987) 242-252

[9] W. J. Karzas and R. Latter, Astrophys. J. Supple. 55 (1961) 167,

[10] S. von Goeler et al., Thermal X-ray spectra and impurities in the ST tokamak, Nucl. Fusion 15 (1975)

[11] http://www.cxro.lbl.gov

[12] http://www.nist.gov/pml/data/asd.cfm

[13] R. L. Boivin et al., Rev. Sci. Instrum. 70, 260 (1999)

[14] http://www.optodiode.com

[15] http://www.analogdevices.com

[16] J.H. Yang, Master thesis, Seoul national university

[17] Martin Mandl, Ph.D thesis, optimization of signal integrity and noise performance of the high density digital links of the TRT readout system

[18] http://www.edmundoptics.com

[19] http:// www.hamamatsu.com

국 문 초 록

VEST 장치에서의 연 엑스선 흡수 박막 방법을 이용한 전자 온도 진단 시스템이 개발 되었다. 연 엑스선 흡수 박막 방법은 서로 두께가 다른 두 장의 박막을 통과한 빛의 세기의 비율을 이용하여 비교적 간단하게 선 평균된 전자온도를 구할 수 있다. 이 방법은 높은 시간 분해능을 가지고 있어서 여러 가지 현상을 진단하는데 도움이 될 수 있고 다른 전자온도 진단 장치의 상호 보완적인 진단 장치로서도 사용될 수 있다.

VEST 장치에서 예상되는 전자온도는 약 100 eV 정도이다. 이 영역대의 전자온도를 측정하기 위해서 0.8 μm and 1.5 μm 두께의 알루미늄 박막이 선정되었다. 이는 전자 온도에 따른 세기 비율과 신호의 세기 변화 계산에 근거 하였다. 각 박막은 플라즈마의 중앙 부분을 진단하기 위하여 VEST 챔버의 중간면에 설치된 검출기들 앞에 위치 하였다. 검출기로는 연 엑스선 영역의 광자에 대해 좋은 검출 성능을 가지고 있는 AXUV-16ELG가 사용되었다. 검출기에서 나오는 각 신호선 들은 전자기적 노이즈를 방지하기 위해 서로 꼬여있고, 구리 그물 전선으로 쌓여 있다.

이 진단 방법은 불순물에 의한 특성 광선과 높은 에너지의 비열적 광선으로부터 영향을 받을 수 있기 때문에, 이러한 광선들이 어떻게 얼마나 발생하는지 아는 것은 중요한 일이다. 계산을 통하여

이들 광선의 영향을 추정하여 보았다. 이 계산을 통해 가장 주요한 불순물 이라고 생각되는 산소의 특성 광선이 있을 경우에는 측정된 전자 온도 값의 범위에 따라 과소 평가 혹은 과대 평가된 전자온도가 예상 되었다. 높은 에너지의 비 열적 광선 들이 있을 경우에는 과소 평가된 전자온도 값이 예상 되었다. 이 광선들의 세기를 가늠해 보기 위해 두 가지 실험 장치가 준비 되었다. 780 nm 주변의 파장의 빛을 통과시키는 필터가 산소 원자의 변화 추이를 측정하기 위해 사용 되었고 추가적인 두꺼운 두께의 알루미늄 박막이 높은 에너지의 비 열적 광선을 가늠하기 위해 사용 되었다. 위 의 계산결과와 두 실험 장치와 더불어 H-alpha line 과 삼중 Langmuir 탐침이 또한 실험결과를 해석하는데 사용되었다.

진단 시스템의 성능을 확인하기 위해 VEST 장치에서 실험을 진행 하였다. 첫 번째 테스트 실험에서 플라즈마 전류가 최대치인 부분에서 약 110 eV 정도의 전자온도가 측정 되었고, 이 값은 플라즈마가 꺼져가는 상황에도 유지가 되었다. 방전의 후반부는 높은 산소 불순물 함량 때문에 측정된 값에 큰 오차가 존재 할 것으로 예상된다.

두 번째 실험은 다른 인자들은 고정된 상태에서 운전 압력과 산소 불순물의 농도가 차이가 나는 두 방전에 대해 진행 되었다. 이 비교에서 두 방전 사이에는 다른 전자온도 값이 예상된다. 측정된 결과에서도 예상되는 방향으로의 전자온도 차이가 존재 하였다.

하지만 2.3 μm 두께의 알루미늄 박막을 사용하여 실험을

진행 했을 때 투과된 빛의 신호는 0.8 μm 과 1.5 μm 두께의 알루미늄 박막에서의 투과된 빛의 신호에 비해 너무 낮게 측정 되었다. 이 값을 바탕으로 전자 온도를 계산 하여 보면 약 20 eV 이하의 값을 나타낸다. 두 번의 실험 사이에서 큰 차이가 존재한다. 낮은 투과된 빛의 신호는 높은 에너지의 비 열적 광선을 가정 할 경우 설명 될 수 있다. 그리고 산소 특성 광선과 높은 에너지의 비 열적 광선의 합쳐진 효과로 측정된 전자온도의 차이를 설명 할 수 있다. 이들 광선에 대한 좀 더 정확한 진단이 마련 된다면 연속 스펙트럼에 대한 이들의 비율이 결정 될 수 있고 좀 더 정확한 전자 온도 진단이 가능 하다.

주요어: 연 엑스선 흡수 박막 방법, 두 박막 방법, 전자온도, 연 엑스선 , VEST, AXUV

학 번: 2012-21012